


N. FANG  
Z. LIU  
T.-J. YEN  
X. ZHANG 

# Experimental study of transmission enhancement of evanescent waves through silver films assisted by surface plasmon excitation

Center for Scalable and Integrated Nanomanufacturing (SINAM), University of California, 5130 Etcheverry Hall, Berkeley, CA 94720, USA

Received: 15 September 2004/Accepted: 23 November 2004  
Published online: 11 March 2005 • © Springer-Verlag 2005

**ABSTRACT** In this paper, we investigated an essential precursor of superlensing: enhancing the transmission of evanescent waves assisted by excitation of surface plasmon. Using natural roughness as a well characterized grating, the transmission of evanescent waves is studied through silver thin films of increasing thickness. Measurements and calculations are performed in the wavelength range of 514.5 nm to 351.1 nm where the real part of the permittivity of silver is negative. Pronounced peaks due to surface-plasmon excitations are observed in the transmission spectra. We found the transmission of evanescent waves rapidly grows with the film thickness up to about 50 nm, after which it decays as loss becomes significant. As the permittivity of a silver slab approaches  $-1$ , we experimentally observed a broadening of surface plasmon bandwidth. Our study indicates a pathway to access the deep subwavelength features by metamaterial superlens.

PACS 42.79-e; 42.30.Wb; 78.20.Ci; 78.66.Bz

## 1 Introduction

The study of light excitation on metal surfaces has been the subject of continuing attention for several decades. However, the realization that a broad spectrum of surface plasmons could be used to reconstruct sub-diffraction-limited image was left unattended until Pendry's recent theory of superlens [1]. Used as a parallel imaging device, Pendry predicted that a thin slab of metal with permittivity,  $\varepsilon = -1$ , has the unique property to regenerate the transmitted evanescent field: the interplay of the near-field object with the surface plasmon excitation of the metal film will compensate for the original decay of evanescent field in optical path, thus forming a transmitted image with diffractionless details.

The fundamental supposition of the superlens, that of evanescent field regeneration, has proved controversial. Yet, we will show experimentally that by studying films of varying thickness, the transmission coefficient of specific evanescent waves can indeed grow up exponentially as a function of thickness under the appropriate conditions. While still far from producing a coherent image, our work provides direct

evidence of the essential foundation of superlensing, and indicates the path that will enable the observation of superlensing at optical wavelengths.

Experimentally, the quantitative and direct measurement of transmission enhancement of evanescent waves has not been reported yet to our knowledge. Most researchers directly take the computed transmission enhancement factor as an input to estimate other physical effects, or indirectly extract the information for the dip in attenuated total reflection. As the evanescent waves in the ideal planar slab superlens do not couple directly with propagating photons, it is necessary to introduce certain coupling mechanism to measure the energy at far field, which perturbs a portion of the original field at interface. Conventionally this can be done with lithographically patterned gratings [2], however, the obtained information would strongly deviate from that of a planar thin film due to the nonlinear coupling efficiency from the highly modulated gratings.

In this work, we quantitatively determined evanescent enhancement in thin metal films by an accurate characterization of the surface roughness with an atomic force microscope (AFM). This allows us to actively employ the random surface roughness of metal films as a natural grating with a plethora of precisely determined Fourier components that scatter light waves in the metal films. The advantage of this method, in comparison to the lithographic gratings, is that the shallow waviness ensures negligible perturbation to the evanescent field, thus a linear coupling scheme is satisfied [3].

In this paper we shall report an investigation of the enhanced transmission of evanescence via surface plasmon excitation. The next section is devoted to a summary of transmission enhancement with the assistance of surface-plasmon. The coupling mechanism of propagating photons with surface-plasmon on a rough surface will be described and the effect of losses will be discussed. The preparation and characterization of the samples is described in Sect. 3. We present in Sect. 4 an experimental study of the sample. We have measured the monochromatic angular scattering profile at fixed wavelengths as a function of the silver film thickness. We have also characterized the surface roughness spectrum of silver films as the thickness varies. Furthermore, we computed the source terms according to the dielectric properties of the silver film. From these results, we are able to obtain the peak transmissivity of the surface plasmon waves as a function of

silver film thickness. The results are compared to theoretical results obtained by means of the Fresnel equation. Moreover, we explore the broadening of surface plasmon bandwidth when we vary the photon energy towards the  $\varepsilon_{\text{Ag}} \sim -1$  condition. Finally, we discuss the issue of experimental errors that will influence the accuracy of the angular transmissivity.

## 2 Theory of surface plasmon assisted transmission enhancement

Instead of resonating with the evanescent waves from the near-field objects for the case of real superlens imaging, in this experiment we make use of the subwavelength surface roughness at silver–air interface to scatter the incident beam and produce EM waves of all possible transverse wavevector  $k_{\parallel}$ . In the following we will demonstrate how the enhanced transmission of evanescent waves can be achieved with the assistance of surface plasmon excitation, and how to estimate the efficiency of coupling between surface plasmon and propagating photons on a rough surface.

### 2.1 Quantitative theory on enhanced transmission

To elucidate how a metallic slab with negative permittivity can enhance the transmission of evanescent waves, we pick up an asymmetric configuration where a thin film of silver is sandwiched between air and glass, and investigate the transmissivity of the  $p$ -polarized evanescent waves across the silver layer. Figure 1a presents the experimental scheme and Fig. 1b shows the asymmetric configuration, whereas Fig. 1c is a realcolor image captured by placing a screen at far field, displaying a double crescent ring, with

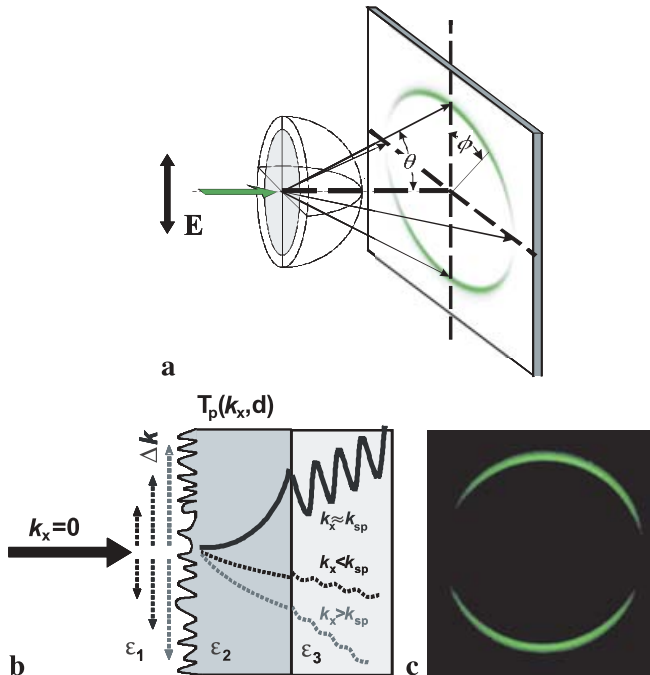


**FIGURE 1** (a) The scattering geometry in experimental setup. (b) The assumed coupling mechanism. The insertion of silver film in optical path generates a strong reflection as well as transmission of evanescent field at air/silver interface due to surface plasmon resonance, thus the overall transmissivity is enhanced. (c) The scattered ring pattern observed at far field

the center of the direct transmitted beam blocked by a circular disk. For a given lateral wavevector  $k_{\parallel} = \sqrt{k_x^2 + k_y^2}$ , we have  $k_{zj} = \sqrt{\varepsilon_j (\frac{\omega}{c})^2 - k_{\parallel}^2}$  for  $j = 1$  (air) and  $j = 3$  (glass); and  $k_{z2} = +i\sqrt{k_{\parallel}^2 - \varepsilon_2 (\frac{\omega}{c})^2}$  for  $j = 2$  (silver). Given a silver slab placed in the region  $0 < z < d$ , we can solve the overall transmission and reflection coefficients using Fresnel equations:

$$T_p(k_{\parallel}, d) = \frac{t_{12}t_{23}}{\exp(-ik_{z2}d) + r_{12}r_{23} \exp(ik_{z2}d)}. \quad (1)$$

Where

$$r_{12} = \frac{\frac{k_{z1}}{\varepsilon_1} - \frac{k_{z2}}{\varepsilon_2}}{\frac{k_{z1}}{\varepsilon_1} + \frac{k_{z2}}{\varepsilon_2}}, \quad r_{23} = \frac{\frac{k_{z2}}{\varepsilon_2} - \frac{k_{z3}}{\varepsilon_3}}{\frac{k_{z2}}{\varepsilon_2} + \frac{k_{z3}}{\varepsilon_3}},$$

$$\text{and } t_{12} = 1 + r_{12}, \quad t_{23} = 1 + r_{23}.$$

The approximation of an exponential growth of the overall transmission  $T_p$  is valid when the following condition  $|r_{12}r_{23}| \gg 1$  is satisfied, that is:

$$\left| \frac{k_{z1}}{\varepsilon_1} - \frac{k_{z2}}{\varepsilon_2} \right| \left| \frac{k_{z2}}{\varepsilon_2} - \frac{k_{z3}}{\varepsilon_3} \right| \gg \left| \frac{k_{z1}}{\varepsilon_1} + \frac{k_{z2}}{\varepsilon_2} \right| \left| \frac{k_{z2}}{\varepsilon_2} + \frac{k_{z3}}{\varepsilon_3} \right| \quad (2)$$

And the overall transmission is in this case:

$$T_p(d) \approx \frac{t_{12}t_{23}}{r_{12}r_{23}} \exp(-ik_{z2}d). \quad (3)$$

In electrostatic limit,  $k_{zj} = ik_{\parallel}$ , and inequality (2) is simplified:

$$|\varepsilon_2 - \varepsilon_1| |\varepsilon_3 - \varepsilon_2| \gg |\varepsilon_2 + \varepsilon_1| |\varepsilon_3 + \varepsilon_2| \quad (4)$$

Assuming both  $\varepsilon_1$  and  $\varepsilon_3$  are loss-free, this only requires

$$-\text{Re}(\varepsilon_2) (|\varepsilon_2|^2 + \varepsilon_1\varepsilon_3) (\varepsilon_1 + \varepsilon_3) \gg 0 \quad (5)$$

A necessary condition of (5) is the real part of  $\varepsilon_2$  being negative.

Furthermore, Inequality (2) implies a diverging reflectivity on either interface, that is,  $\left| \frac{k_{z1}}{\varepsilon_1} + \frac{k_{z2}}{\varepsilon_2} \right| \left| \frac{k_{z2}}{\varepsilon_2} + \frac{k_{z3}}{\varepsilon_3} \right| \rightarrow 0$ . This is exactly the case of surface plasmon resonance on either side of the slab, where the normal component of  $E$ -field across the interface are equal and opposite. We should note that the enhanced transmissivity is independent of the surface on which the surface plasmon is excited.

### 2.2 Coupling due to surface roughness

Surface plasmons are collective excitations of electron plasma at a surface of metal coupled with photons. They are characterized by the wave vector  $k_{\text{sp}}$  exceeding the wave vector of propagating photons of the same frequency in vacuum ( $k = \omega/c$ ) and, therefore, cannot be excited directly by light on a perfectly smooth surface. In the following section, we will discuss how to utilize the random roughness of silver to scatter the incident beam and convert the propagating wave

to evanescent field with all possible spatial modulations, characterized by a transverse wavevector  $k_{//} > 2\pi/\lambda$  in Fourier spectrum. These evanescent waves permeate the silver film. And when  $k_{//} < 2\pi n_p/\lambda$ , ( $n_p$  is the refractive index of the prism), they are converted back to propagating waves, so we can measure the transmissivity of each evanescent mode at far field.

Here, following the treatment of [4, 5], we approximate the rough surface of a small waviness by introducing an inhomogeneous scattering layer at metal-vacuum interface that linearly perturb the original field. In general, the polarization current induced by the incoming electromagnetic field can be decomposed of three components in  $x, y, z$ , each acting as a Hertzian dipole on metal surface. Given a surface corrugation  $z = s(x, y)$ , and its Fourier transform reads:

$$S(\mathbf{k}_{//}, 0) = S(k_x, k_y, 0) = \iint s(x, y) \exp(ik_x x + ik_y y) dx dy. \quad (6)$$

Let  $E_{1,2}^{(0)}(\mathbf{k}_{//}, z)$  be the original fields in the  $\varepsilon_1, \varepsilon_2$  medium separated with flat interface, given by the conventional Fresnel equations. Specifically in our case, with the incident beam  $\mathbf{k}_{//}^{(0)} = 0$ ,  $\varepsilon_1 = 1$  and  $E_{1,2}^{(0)}(\mathbf{k}_{//}, z)$  in the direction of  $(1, 0, 0)$ , the surface corrugation induced current approximates to:

$$\mathbf{J}(\mathbf{k}_{//}) = i\omega S(\mathbf{k}_{//}) \left( \frac{\varepsilon_2 - 1}{4\pi} E_2^{(0)}(\mathbf{k}_{//}^{(0)} = 0, 0) \right), \quad (7)$$

and with  $k_{zi} = \sqrt{\varepsilon_i - \varepsilon_3 \sin^2 \theta}$ , the  $H$  field advancing in  $z > 0$  direction is given by

$$\mathbf{H}(\mathbf{k}_{//}, z) = \frac{(\mathbf{k}_{//}, k_{z2})}{i4\pi k_{z1}} \frac{k_{z1}}{\varepsilon_2 k_{z1} + k_{z2}} \times \mathbf{J}(\mathbf{k}_{//}) \exp(ik_{z2}z) \quad (8)$$

Since in our case the  $E_{1,2}^{(0)}(\mathbf{k}_{//}, z)$  is in the direction of  $(1, 0, 0)$ , we have  $J_z = 0$ , and specially at  $\varphi = 0$ , we have  $\mathbf{k}_{//} = k_x$ ,  $\vec{J}(\mathbf{k}_{//}) = J_{//}(1, 0, 0)$ . For the  $p$ -polarized field amplitude, the resulting  $H$  field that radiate to  $+z$  direction in the  $\varepsilon_3$  medium reads [5]

$$\begin{aligned} H_p(k_x, z) &= \frac{\exp(ik_{z3}(z-d))}{4\pi k_{z1}} \frac{k_{z1}}{\varepsilon_2 k_{z1} + k_{z2}} \\ &\times \frac{1}{\varepsilon_2 + 1} \omega S(k_x) \frac{\varepsilon_2 - 1}{4\pi} E_1^{(0)} T_P(k_x, d). \end{aligned} \quad (9)$$

This yield to the scattered far-field light intensity  $dI_p$  per solid angle element  $d\Omega_z$  normalized by incident intensity  $I_0$ , as given by the following:

$$\begin{aligned} \frac{dI_p}{I_0 d\Omega_3} \Big|_{\varphi=0} &= \frac{1}{4} \left( \frac{\omega}{c} \right)^4 |S(\mathbf{k}_{//}, 0)|^2 \\ &\times |T_P(\mathbf{k}_{//}, d)|^2 |W_p(\theta, \varphi = 0)|^2; \end{aligned} \quad (10)$$

with [2, 6]

$$W_p(\theta, \varphi = 0) = \frac{4}{\varepsilon_2 + 1} \frac{(\varepsilon_2 - 1) \sqrt{\varepsilon_2 - \varepsilon_3 \sin^2 \theta} \sqrt{1 - \varepsilon_3 \sin^2 \theta}}{\left( \varepsilon_2 \sqrt{1 - \varepsilon_3 \sin^2 \theta} + \sqrt{\varepsilon_2 - \varepsilon_3 \sin^2 \theta} \right)} \quad (11)$$

Please note that (10) implies the scattering only occurs once at the air/metal side, while the roughness at the metal/prism interface and the scattering inside metal films does not contribute to the collection of evanescent waves. This single scattering approximation has limitations; yet according to [5], the internal scattering due to bulk inhomogeneities of silver films will mainly emit the light of irradiative plasmons ( $\text{Re}(\varepsilon_{Ag}) \sim 0$ ), whereas the surface roughness is responsible for the light from nonradiative plasmons ( $\text{Re}(\varepsilon_{Ag}) \leq -1$ ). Furthermore, the angular dependence of the scattered light in both cases is rather different and allows one to discern between interior and surface roughness. These results are important to evaluate the experiments with scattered light.

### 2.3 Dispersion and damping due to surface roughness

In order to realize a perfect lens, the allowed bandwidth of  $k_{//}$  for the enhancement of evanescent wave in the medium should extend to infinity. However, in real metallic films, there exists finite bandwidth of  $k_{//}$  in which enhancement can be realized [7–9]. Arakawa et al. [10] and Alexander et al. [11] were among the first to suggest that surface plasmon interactions be characterized by a complete response function surface rather than by a single dispersion curve. In fact, when experiments are performed by scanning over the wavenumber  $k_{//}$  at a fixed real frequency  $\omega$ , the peak position of transmissivity presents the real part of the surface plasmon wavenumber while the width presents its imaginary part. This width contributes to the available bandwidth  $k_{//}$  for enhancement. As  $\text{Re}(\varepsilon_2(\omega)) \rightarrow -\varepsilon_1$ , (4) is satisfied for a large spectrum of transverse wavevectors, and the largest bandwidth for enhanced transmission can be achieved.

The geometrical deviation of the rough surface from a perfect plane perturbs the surface plasmons and it is natural to expect a change in the dispersion relation [2]. Prior experiments [12, 13] and theory [14] on the attenuated total reflection showed that both the displacement  $\Delta k_{sp}$  and the width broadening of wavevector  $\delta k_{sp}$  increases with a growing roughness of the surface. In fact to quantify both effects, double scattering or higher order processes on the rough surface have to be taken into account. In [3, 14] it is shown that in the case of slightly wavy surfaces, both  $\Delta k_{sp}$  and  $\delta k_{sp}$  are proportional to the surface roughness  $|S(k_{sp,0})|^2$ .

## 3 Sample preparation and experimental setup

In our experiments, silver films with thickness ranging from 30 to 90 nm were deposited onto BK7 hemispheres using a programmable e-beam evaporator (SLOAN SL 1800). The evaporation rate was set to  $1 \text{ \AA/s}$ , with base pressure  $< 3 \times 10^{-6}$  Torr. The film thickness is chosen to be larger than 30 nm, ensuring that the bulk optical properties of silver can be applied in the calculations [15]. The surface property of BK7 and the deposited silver films will be presented in Sect. 4.

To gain some insight of the film microstructures at current deposition condition, we performed cross-sectioning transmission electron microscopy (TEM) on 50 nm thick silver film. As shown in Fig. 2, no apparent voids and volumetric cracks are observed. This supports our assumption in Sect. 2

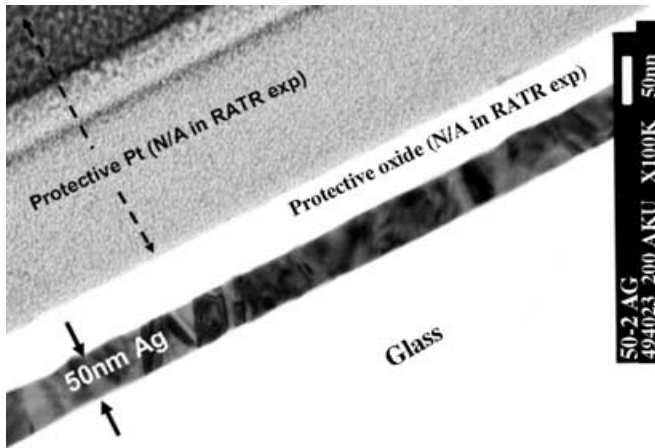


**FIGURE 2** Transmission electron microscopy of cross-sectioned 50 nm silver film. It can be seen that the air/silver interface (*upper part*) is slightly wavy but not highly modulated within a correlation length of 100 nm

that contributions from bulk inhomogeneities in silver are insignificant to the scattered intensity.

To measure the relative transmission enhancement of the evanescent waves, we used a reversed attenuated total reflection (RATR) scheme [16]. A collimated  $\text{Ar}^+$  ion laser beam with wavelength  $\lambda$  and diameter  $< 1.5$  mm illuminates the sample surface from the air side with normal incidence (Fig. 3a). The mounted hemisphere samples are leveled and centered with micro-actuators with  $10 \mu\text{m}$  resolution to ensure concentricity better than  $300 \mu\text{m}$ . A  $1/3$  inch charge-coupled device (CCD) camera is placed about 5 cm away from the center of BK7 prism to measure the relative light intensity along the azimuthal angle  $\theta$ , while  $\varphi$  is centered at zero. For these samples with different thickness, we tune the variable attenuator to adjust the input laser power  $I_0$ , so that the power of transmitted light cone falls in the linear dynamic range of the CCD camera. To further enhance intensity resolution, the intensity profiles captured by CCD are averaged in  $-3^\circ < \varphi < 3^\circ$  direction. The angular resolution and repeatability in the setup is calibrated to within  $0.1^\circ$ .

In Fig. 3b, we display a typical angular profile of measured scattered intensity by varying sample thickness. We can observe a remarkably strong intensity peak around  $46\text{--}48$  degrees, which indicates the excitation of surface plasmon at wavelength of  $514.5$  nm. Note that in Fig. 3b, the maximum of the scattered intensity are offset by range of  $\pm 0.5^\circ$  for the samples of different thickness, which are primarily attributed to the commercial prisms that are slightly different from hemispheres. We will verify this conclusion in Sect. 5.

In our system, the  $\text{Ar}^+$  laser can provide seven different emissions ranging from  $514.5$  nm to  $351.1$  nm. This readily gives us the freedom to explore the broadening of transmission enhancement as the permittivity of silver move up from  $-10.7$  ( $514.5$  nm) towards  $-1.5$  ( $351.1$  nm). Figure 4 displays the scattered intensity through a  $50$  nm thick silver film for different incident wavelength. To calibrate the sensitivity of CCD, the input intensity is adjusted and monitored for different emission wavelengths, in the range of  $10\text{--}80$  mW with an output variation less than  $0.5$  mW. The quantitative interpretation of these data will be left until Sect. 5.

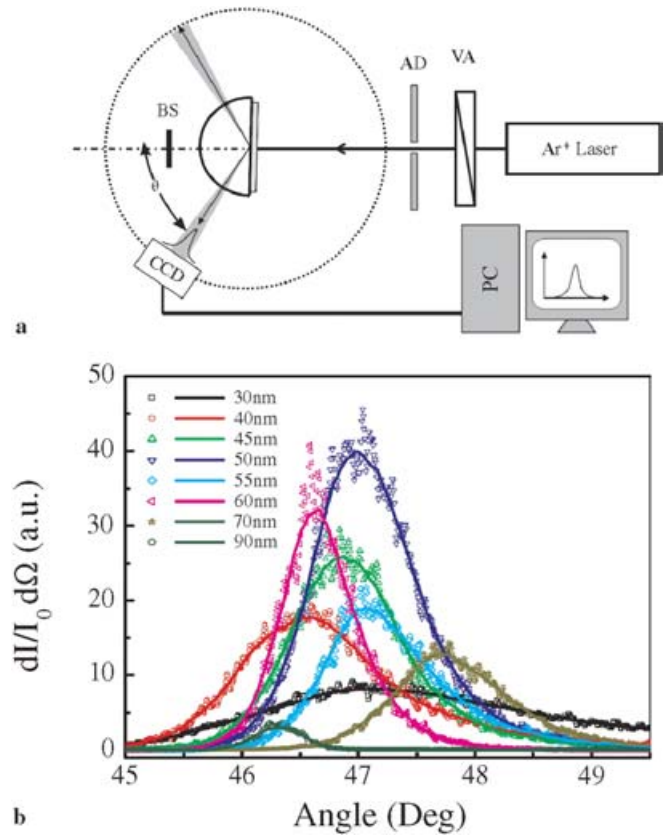


**FIGURE 3** (a) RATR setup to measure the relative transmissivity of evanescent waves. The direct transmission at the center of the ring is blocked by a mask. AD: aperture diaphragm, VA: variable attenuator, BS: beam stopper. (b) The measured scattered intensity profile versus azimuthal angle  $\theta$  at  $\varphi = 0$ . The illumination wavelength  $\lambda = 514.5$  nm

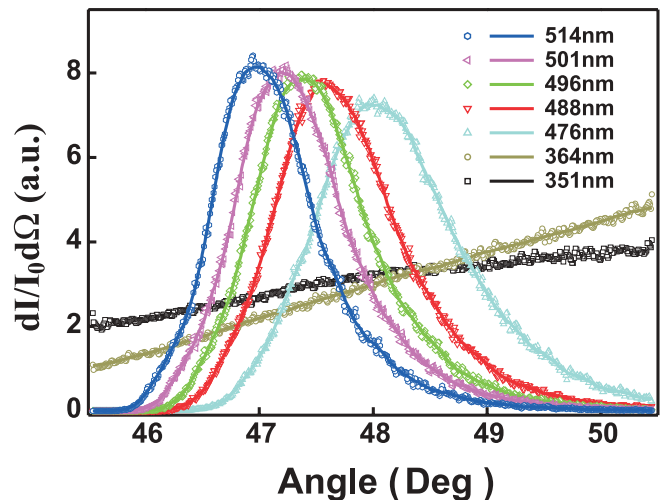


**FIGURE 4** The angular profile of scattering intensity of  $50$  nm silver film sample as a function of varying wavelength.

#### 4 Characterization of surface roughness

Conventionally, the natural roughness is mainly considered as a noise that spread the surface waves which complicate the validation and reduce the measurement accuracy. Limited by the available experimental methods, the early estimation of surface roughness parameters is typically

extrapolated from either a Gaussian or exponential decaying model, without further careful justifications [2]. A few literatures are found in the study on thickness dependence of enhanced light emission efficiencies [17], but the artificially enhanced film roughness was not quantized and only an integrated intensity signal was given. However, as the surface properties vary with silver films of different thickness, we will show that a simple extrapolation of the surface roughness would likely result in a fragmented and obscure picture of the transmission enhancement.

In our experiment, we quantitatively characterized the surface roughness of our sample on a commercial atomic force microscope (Dimension 3100, Veeco Digital Instrument). For mapping all the samples we employed tapping mode probes (NCH-20, Nanosensors) with an acute cone angle of  $20^\circ$  and radius of curvature better than 10 nm. The growth condition permits a root-mean-square (RMS) roughness  $< 2.5$  nm on the evaporated silver samples, while on the BK7 glass the RMS roughness is less than 0.5 nm. These conditions are adequate for our previous assumption of slightly wavy surface and weak scattering on the air/silver interface.

Since the spectral resolution  $\Delta k_{//}$  is inversely proportional to the diameter of the scanned sample, a large scanning area is preferable. Thus for each sample a square of  $60 \mu\text{m} \times 60 \mu\text{m}$  was profiled and digitized with  $512 \times 512$  sampling steps. By taking 2D-Fourier transformation of the surface profile, we then averaged the radial roughness spectrum of 50 nm silver sample as shown in Fig. 5. It turns out that such surface roughness profile does not follow neither a theoretical Gaussian nor exponential functions. At correlation lengths ranging from 300–600 nm, the spectrum strength is relatively flat instead of decaying with increased wavevectors. In fact it is not surprising because the growth method and substrate materials can significantly influence the microstructure of silver films [15].

The measurement errors are taken from the standard deviation of the statistical data, typically around 10%–20%. As we will show later, this contributes to the major error in our estimation of the transmissivity. The surface roughness characteristics as observed from AFM and TEM (Fig. 2) are in good agreement (deviation  $< 10\%$ ) at the wavevector  $k_x$  of interest (300–600 nm in period), indicating the accuracy of  $|S(k_x)|^2$ .

To further demonstrate the important fluctuation of surface roughness spectrum as film thickness varies, the relationship of the Fourier transformed surface roughness  $|S(k_{sp})|^2$  versus silver film thickness are plotted in Fig. 6. It can be seen that the specific spectrum strength at 514.5 nm can vary up to 50% in different sample thickness even when the growth condition are similar. Therefore, we can conclude that a careful justification of  $|S(k_{sp})|^2$  in samples with increasing thickness is the key to a reliable extraction of enhancement factor  $|T_p|^2$  from (10).

Since the sample spot under laser beam is 1.5 mm, while the surface area we probed using AFM is much smaller, it is natural to ask how reliable is the statistical sampling process. To verify that, we have randomly selected different areas of the same silver film and repeated the surface profiling with  $30 \mu\text{m}$ , as shown in Fig. 7. The results from 4 sampling areas are in very good agreement, and the standard deviation resulting from the statistical processes are again within the tolerance of 20%.

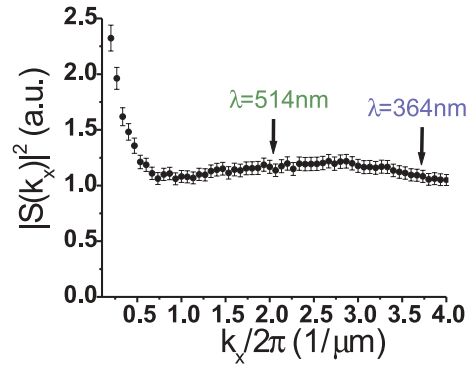


FIGURE 5 The extracted surface roughness spectrum of 50 nm silver film. The arrows indicate the corresponding surface plasmon wavevector at corresponding wavelengths.

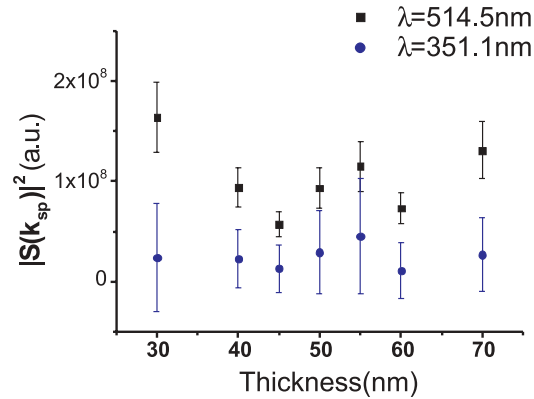


FIGURE 6 The extracted surface roughness spectrum  $|S(k_{sp})|^2$  as a function of sample film thickness. The black square and blue circles corresponds to wavelength 514.5 nm and 351.1 nm, respectively

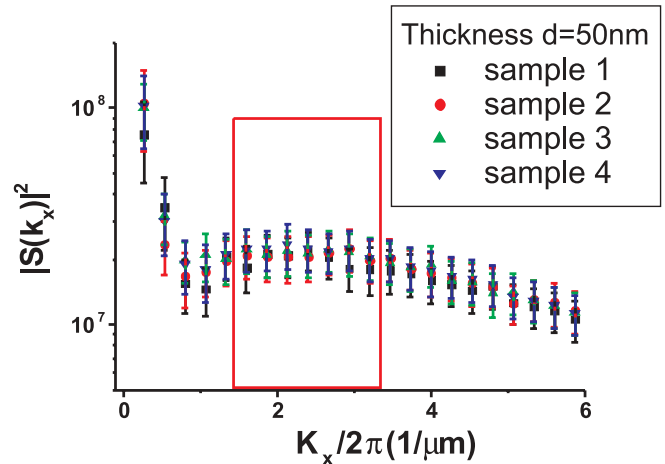
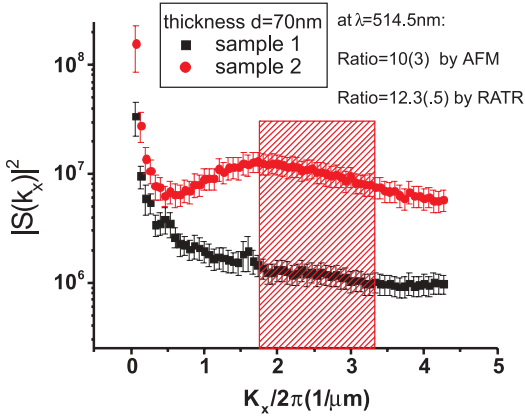


FIGURE 7 The statistical sampling of  $|S(k_x)|^2$  with four different areas on the same 50 nm silver sample. The red rectangle indicates the data corresponding to the excitation wavelengths of interest.

Finally, from (10), we can conclude that for samples of same thickness but with different roughness characteristics, the corresponding scattered intensity should be proportional to the specific roughness spectral strength  $|S(k_{sp})|^2$ . To validate this finding, we prepared 2 samples of 70 nm films by slightly changing the deposition base pressure. The difference in deposition conditions gives rise to two distinctive surface roughness spectrum as shown in Fig. 8. At wavelength of



**FIGURE 8** The statistical sampling of  $|S(k_x)|^2$  with 2 samples of 70 nm silver sample with slightly different deposition base pressure. The resulting surface roughness is distinct between the two samples, with about ten times difference in the strength of  $|S(k_{sp})|^2$  at 514.5 nm. This is verified by the ratio of scattered intensity

514.5 nm, the ratio of the two surface roughness  $|S(k_{sp})|^2$  yield  $10 \pm 3$ , which is in good agreement with the measured ratio in corresponding scattered intensity ( $12.3 \pm 0.5$ ). This confirms the accuracy of our measured surface roughness spectrum.

In summary of this section, we found that the significant variation of surface topology in samples of different thickness do not support the assumption of Gaussian or exponential function of surface roughness spectrum. An oversimplified and arbitrarily extrapolation of roughness parameters will potentially swamp the estimated transmission within noise, resulting in irreproducible data as those reported in [17]. Instead, with accurate characterization of the surface roughness, we can actively employ the random surface roughness of metal films to estimate the coupling strength of surface plasmons with propagating photons.

## 5 Experimental and theoretical analysis of the enhanced transmission band

### 5.1 The extraction of transmissivity

The analysis of the presented angular profile of scattered intensity clearly indicated the enhanced transmis-

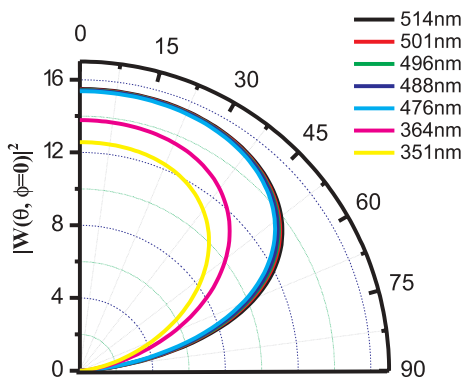


**FIGURE 9** The computed dipole function using (5.11). The permittivity  $\epsilon_2$  of silver is taken from [18], while the dispersion of refractive index of BK7 is from [19]

sion with the assistance of surface plasmon. In order to fully characterize the transmissivity of the silver films as the thickness increases, it is therefore necessary to obtain the appropriate dipole function in addition to the measured surface roughness spectrum. In Fig. 9, we computed the dipole function  $|W(\theta, \varphi = 0)|^2$  using the theoretical values from (11), with the dielectric properties of silver and BK7 provided by [18, 19], respectively. In fact the dipole terms expands with larger divergence angle when  $\text{Re}(\epsilon_{Ag})$  take very large negative values, as in the case of 514.5 nm ( $\text{Re}(\epsilon_{Ag}) \sim -10.7$  from [18]), while

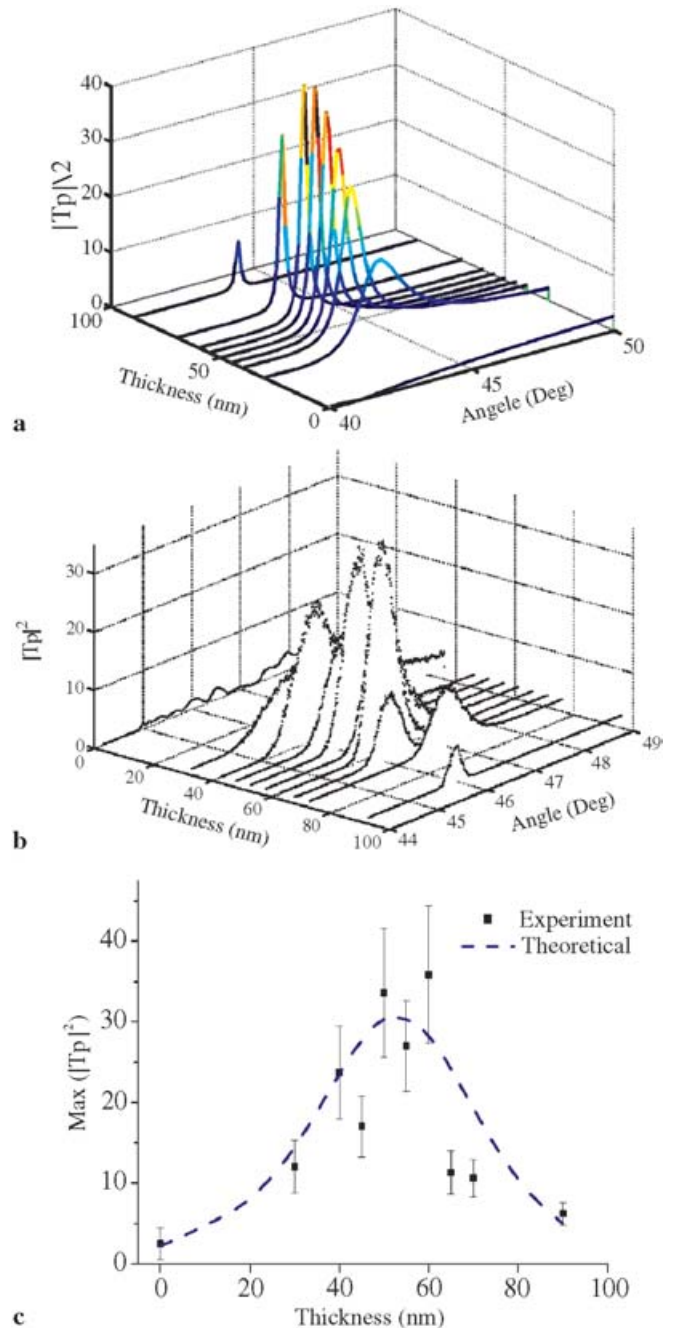


**FIGURE 10** (a) The computed  $|T_p|^2$  and (b) the measured  $|T_p|^2$  as a function of film thickness and angle.  $\epsilon_y = -10.7 + 0.42i$ ,  $\lambda = 514.5$  nm. (c) The measured enhancement factor as a function of silver film thickness. The theoretical curve is computed using the Fresnel equation with  $\epsilon = -10.7 + 0.42i$  (Imaginary part fitted from experiment)

the field strength is smaller at grazing angles when  $\text{Re}(\epsilon_{Ag})$  approaches  $-1$ . This also setup a constrain of the observable wavevectors; practically the azimuthal angle is less than  $70^\circ$  as in our experiments.

Using (10), we then successfully extracted the enhanced transmissivity  $|T_p|^2$  as a function of sample thickness (Fig. 10b) based on the results of Figs. 3b and 9. Because we do not have absolute unit in photon counting  $dI/d\Omega$  as well as the Fourier transformed roughness spectrum  $|S(k_x)|^2$ , a calibration of reference unit is necessary. This is done by measuring the max  $|T_p|^2$  at 0 nm (bare BK7 glass hemisphere) as a reference in the measurement window. The theoretical value is 2.31 at  $48^\circ$  on the reference when we use wavelength at 514.5 nm; therefore, we can normalize the maximum of

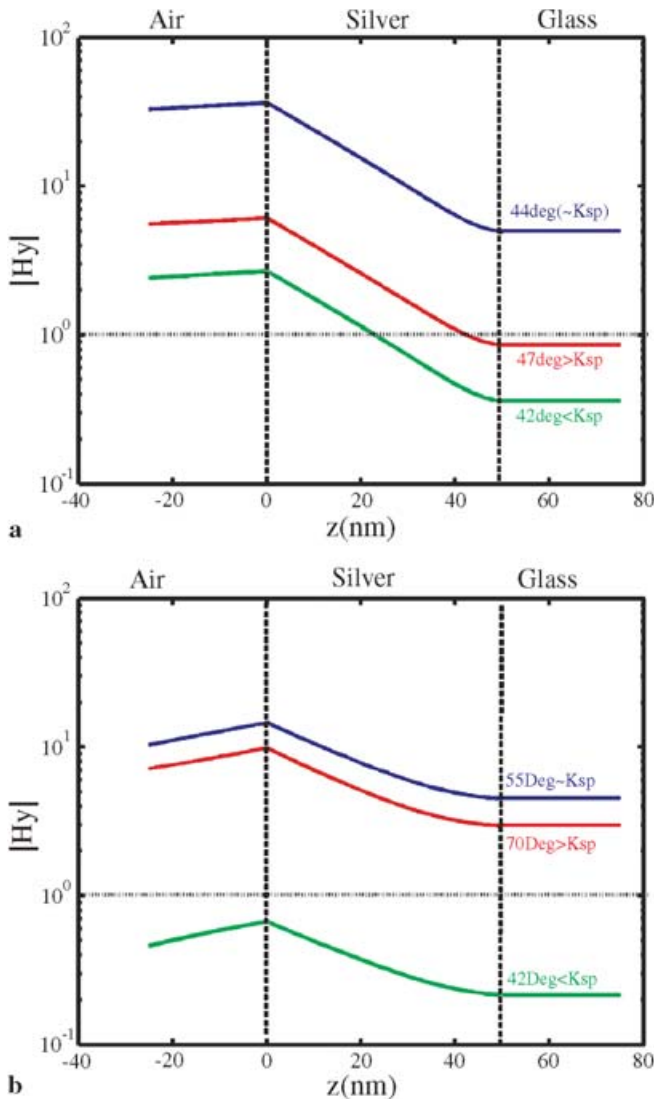


**FIGURE 11** (a)  $H_y$  field distribution across the silver film,  $\lambda = 514.5$  nm,  $\epsilon_{Ag} = -10.7 + 0.4i$ , slab thickness  $d = 50$  nm. The dotted line indicates the original field strength, and we can find although the field decays inside silver film, at surface plasmon resonance angle ( $k_{sp}$ ), the high reflectance of metal elevate the effective field strength at air side. Therefore, after decaying through metal film, we still obtain an enhanced transmission (the factor  $|T_p|$  is larger than five); while above or below resonance angle, the transmission factor is less than one. (b)  $H_y$  field distribution across the same 50 nm silver film,  $\lambda = 351.1$  nm,  $\epsilon_{Ag} = -1.5 + 0.28i$ . In this case a broad bandwidth is found with enhanced transmissivity larger than unity

measured ratio  $\frac{dI}{d\Omega} / |S(k_x)|^2 |W(\theta, \varphi = 0)|^2$  over  $42^\circ$  to  $48^\circ$  to this value. In comparison, in Fig. 10a we plotted the theoretical transmissivity as a function of silver thickness, with the dielectric properties of silver and BK7 taken from literature [18, 19]. From Fig. 10a and b we can see the good agreement of the peak shapes and strengths; however, a systematic shift of peak position (about  $2^\circ$ ) is identified, which are attributed to the deviation of the glass prism from perfect hemispheres.

In Fig. 10c, the peak values are selected in replacement of the values corresponding to each  $k_x$ , mainly to remove the peak shift in  $k_x$  which may occur due to possible aspherical deformation of each prism from fabrication variations. We found that the enhancement factor  $|T_p|^2$  rapidly grows with increasing silver thickness up to 50 nm. Although not previously viewed as significant in metal optics theory, this is actually an important effect that builds the foundation of supersensing.

As we mentioned, in our experiment only the surface plasmon at first surface (air/silver) is excited, while the magnetic field decays into metal layer. As elaborated in Fig. 11, even with decaying tail, the magnetic field strength at exit is already higher than that of a pure dielectric scattering layer, which

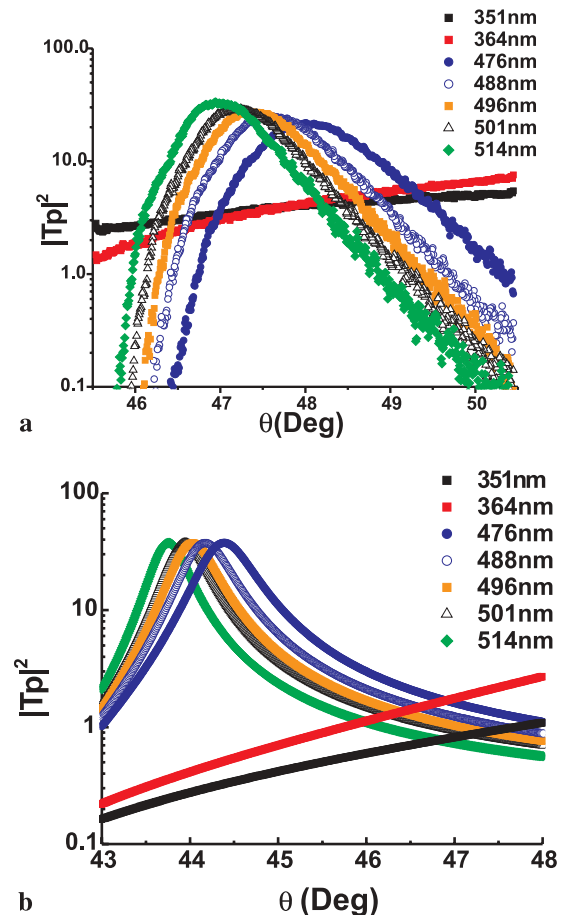


**FIGURE 12** (a) The angular profile of the measured transmissivity of a 50 nm silver film as a function of varying wavelength. The azimuth angle corresponds to  $k_x = \frac{\omega}{c} n_p \sin \theta$ . In this wavelength range from 514.5 nm to 351.1 nm, the real part of silver permittivity,  $\text{Re}(\epsilon_{Ag})$ , changes from  $-10.7$  to  $-1.5$ . (b) The computed transmissivity of 50 nm silver film as a function of wavelength

gives rise to a transmissivity larger than unity. When the metal film thickness increases, the transmissivity can further grow up by the constructive coupling [1, 2] of the surface plasmons with the irradiative waves at glass/silver interface (Fig. 1b), which in turn elevates the overall field strength at first surface. Above 50 nm, as the surface modes at two interfaces start to decouple, the enhancement is suppressed by the intrinsic loss inside the metal film [20]. As a consequence, the transmissivity decays as film thickness further increases. For the first time to our knowledge, our experimental results provide direct evidence of the thickness dependence of enhanced evanescent field across the silver film, a key prediction in Pendry's superlens theory [1]. If switching the surface roughness back to the near-field object, then it is essential in this case that the silver film matches the evanescent waves from the object. This can be done by coordinating the surface current distributions at the silver/glass interface, thus enhance the amplitude of the transmitted near-field.

Concurrent to examining the transmissivity of evanescent waves as a function of growing film thickness, we obtained the wavelength dependence of the resonantly transmitted evanescent modes, more specifically the allowable bandwidth. At  $\lambda = 514.5$  nm, we find  $|T_p|^2 > 1$  for a range of  $\theta = 46\text{--}49^\circ$ , which corresponds to  $k_x = 1.09\text{--}1.15k_0 (= 2\pi/\lambda)$ . As displayed in Fig. 12a, by decreasing the wavelength  $\lambda$  from 514.5 nm to 351.1 nm ( $\epsilon(\omega) \rightarrow -1$ ), we can clearly observe a remarkable bandwidth broadening of amplified  $k$  spectrum, accompanied by a remarkable shift of resonant peak towards larger angle  $\theta$  as  $k_{sp}$  increases with decreasing  $|\epsilon|$ . At  $\lambda = 351$  nm, where  $\epsilon_{Ag} = -1.5 + 0.27i$ , we observed that the bandwidth of amplified evanescent wave spectrum approaching to a measurable range of  $1.02k_0 < k_x \leq 1.44k_0$  (the upper limit is set by the cutoff of dipole function at about  $70^\circ$ ). The measured expansion of bandwidth is in good agreement with theoretical calculations in Fig. 12b, which provides a design base to improve the accessible bandwidth for the superlens imaging.

## 5.2 The influence of overlayer to the measurement accuracy

Throughout this paper, the measurement accuracy of the transmissivity is our emphasis. Besides the statistical error of the surface roughness spectrum, there are certainly additional factors that affect the quantitative picture of transmission enhancement. In order to justify that the overall error is mainly from the contribution of the statistical deviation, here we pick up the influence of possible surface contamination and estimate the possible systematic error in our experiments.

Since the silver samples are exposed to the ambient environment during AFM mapping and light scattering experiment, it is possible that a very thin skin of silver film is oxidized by  $O_2$  or  $H_2S$ . Such overlayer is self-passivating and yield a typical thickness of 1–2 nm [21]. Meanwhile, the condensation of water moisture could also create an overlayer onto the silver films. Without loss of generality, here we take the water overlayer as an example to elaborate its influence to our measurement. The introduction of the dielectric overlayer directly affects two factors in our experimental analysis: first,

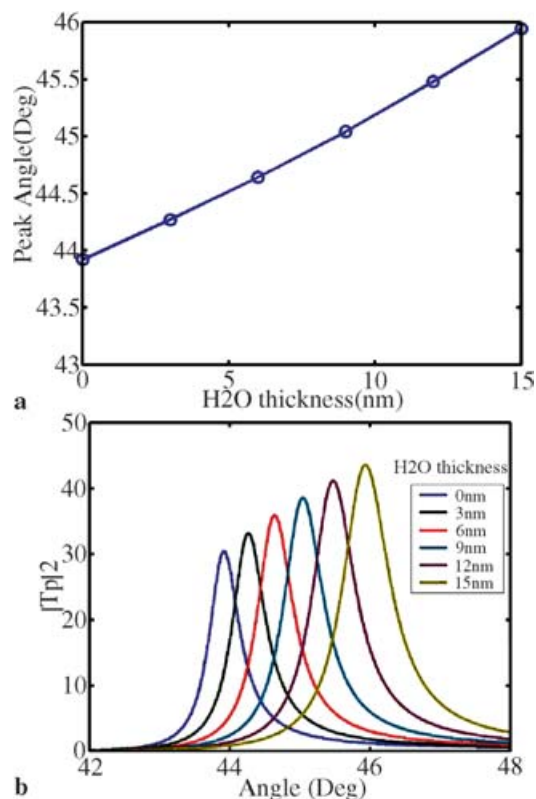


**FIGURE 13** The simulated (a) peak position and (b) transmissivity of a 50 nm silver film with a thin overlayer of water moisture. It is evident that the peak linearly shifts to a larger angle with an increasing overlayer thickness

the peak shift; and second, the correction to dipole function. Finally, in the theoretical estimation, the insertion of a fourth medium can be modeled with standard layered structures and an overall transmission is given numerically.

**5.2.1 The peak shift.** The possible assignment of peak shift in our experiment is not free from ambiguity. Besides the reason of manufacturing error of the hemispheres, the overlayer can be a possible cause [3]. Such shift is proportional to the overlayer thickness  $d'$ . For a 50 nm thick Ag film and wavelength of 514.5 nm, the theoretical peak shift due to  $H_2O$  absorption is shown in Fig. 13. As the moisture overlayer increased up to 3 nm, we could observe a shift of 0.4 degree towards larger angle. This is more significant with  $Ag_2S$  and  $Ag_2O$  contamination, because these materials attain higher dielectric constant ( $\epsilon = 6\text{--}9$ ) compared to water ( $\epsilon = 1.77$ ). The constitution of chemical contaminant will be investigated in future works.

**5.2.2 The influence to dipole function.** From Sect. 2, we can observe that the placement of the scattering layer is sensitive to the dielectric environment. Due to the existence of water coating, the scattering due to roughness is now bounded to the interface between silver and water. A simplified way of correction in the dipole function is then to replace the permittivity of silver and glass with that of  $\epsilon_{Ag}/\epsilon_{H_2O}$  and  $\epsilon_{BK7}/\epsilon_{H_2O}$ . As a consequence, the dipole function  $|W(\theta, \varphi = 0)|^2$  is lowered. For example in  $\lambda = 514.5$  nm, the introduction of water layer will lower the dipole term from 14.56 to 13.84 at  $\theta = 48^\circ$ . The



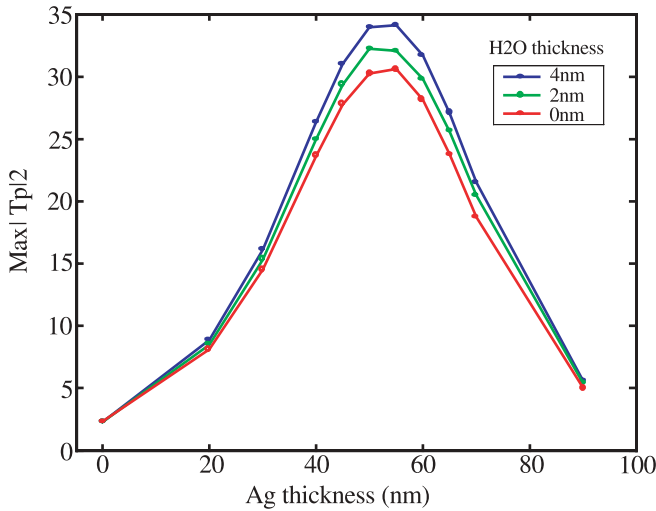


**FIGURE 14** The numerically computed increase of transmissivity of evanescent waves due to the existence of water overlayer

systematic error of the dipole function over 44–49° is within (–5%). In general, the effect of overlayer reduces the strength of dipole term in forward directions, because it is now possible to couple the scattered field to some guided mode in the overlayer.

**5.2.3 The influence to transmission enhancement factor.** The introduction of water layer reduces the reflection at first surface, therefore the transmission enhancement factor is increasing with increasing water film. As shown in Fig. 14, when water film thickness increases from 0 to 4 nm, our estimation using the four layer configuration shows that the peak transmission factor  $|T_p|^2$  at film thickness 50 nm increases from 30.3 to 33.8 (+10% increase). In general, the introduction of dielectric overlayer will alter the reflectance of first interface, and the broadening of the enhanced transmission peak would occur at longer wavelength. Since at 351 nm we still can find a significantly enhanced transmission band, our result in Fig. 12a does not support the tractable overlayer of  $\text{Ag}_2\text{S}$ . On the other hand, due to the limited selection of wavelengths in our experiment, we cannot exclude the presence of water condensation.

From the above estimation on the influence of overlayer, we can conclude that neglecting this overlayer will lead to a maximum of 10% systematic error. This is still smaller than the statistical sampling error ( $\sim 20\%$ ) we mentioned in AFM surface profiling process. Therefore, we can safely assign the major error to the statistical sampling.

### 5.3 On the peak shift and spreading due to surface roughness

In Sect. 2, we introduced the effect of surface roughness to the displacement of transmission resonance and spreading of transmission. From the estimation of the width of the transmission peaks in Fig. 10b, we can estimate the propagation length of surface plasmons to be in the order of 10–50 wavelengths, sufficient for multiple scattering of these surface plasmons to occur on the rough air/silver interface. If taken into account the multiple scattering terms, we must be able to

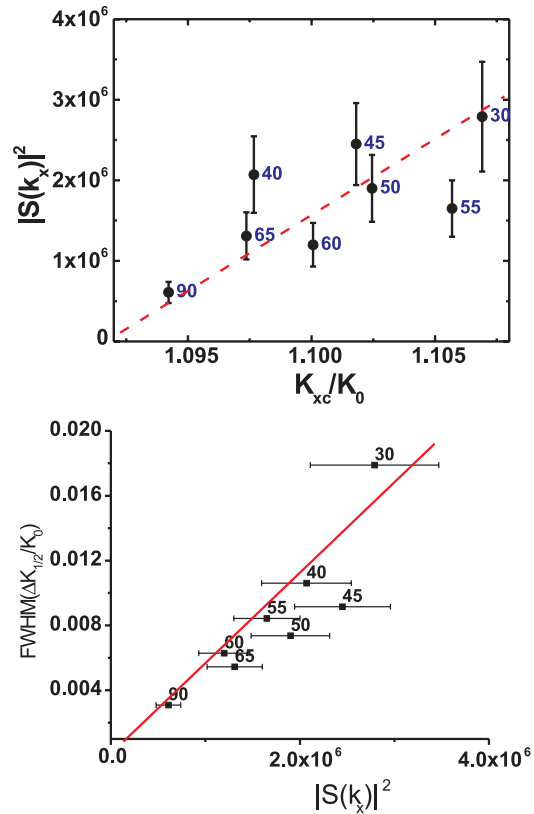


**FIGURE 15** The measured (a) displacement and (b) broadening of the transmission peaks as a function of characterized surface roughness spectrum. The red lines are guided by eye. The data labels indicate the thickness (in nm) of silver films. In (a) the abscissa  $K_{xc}/K_0$  denotes the central peak position normalized by vacuum wavenumber, where in (b) the y-axis (FWHM ( $\Delta K_{1/2}/K_0$ )) defined as the fitted full width at half modulation of the transmission peaks normalized by vacuum wavenumber

establish a linear relationship on the spectral strength of specific surface roughness  $|S(k_{sp})|^2$  with the displacement and broadened width of enhanced transmission peak.

Using the results of Fig. 10b, we can plot the position and the fitted width of resonance peaks as a function of surface roughness  $|S(k_{sp})|^2$ . As shown in Fig. 15a and b, we can observe to some extent the linear correlation of the surface roughness spectrum and the corresponding displacement and broadening in transmission peaks. This observation again validates our assumption of weak scattering from slightly wavy surfaces.

## 6 Summary and concluding remarks

The rapid growth of evanescent waves assisted by the surface plasmon excitation brings a novel pathway to diffraction-free imaging. Used as an imaging device, a thin film of negative permittivity material can resonate with a band of evanescent waves of the near-field object and transfer them to the further side without losses. As the permittivity of the material matches with the surrounding medium, it is possible to couple a wide band of evanescent modes and regenerate them at image plane, thus realizing a diffraction-free superlensing.

In order to design and engineer a superlens with high transmissivity and large bandwidth, it is necessary to study

the interplay of the evanescent waves with surface plasmons. We have studied experimentally the enhanced transmission of evanescent waves assisted by excitation of surface plasmons. An enhanced transmissivity of evanescent wave through a silver film is extracted by exciting them through natural surface roughness and by analyzing the dipole radiation characteristics of the surface scatterers. The transmissivity bandwidth broadens apparently when the surface plasmon excitation frequency approaches its resonance frequency. This opens the gateway to access the subwavelength features of a near-field object by synthesizing the enhanced evanescent components with the help of surface plasmon excitation. To our knowledge, this is the first direct and quantitative measurement of transmissivity of evanescent waves as a function of increasing film thickness and decreasing wavelength. It is a major result of this paper showing that a full characterization of surface roughness allows one to quantitatively describe these phenomena. Although these experiments are conducted with pristine silver films, the experimental configuration will provide a testbed for the artificially synthesized metamaterials.

Finally, we have discussed the fundamental issue of measurement accuracy in our experiment. We have used a weak scattering theory to provide a general framework that allows one to interpret mechanism of coupling propagating photons with surface plasmons. In particular, we have experimentally verified that a linear correlation can be found between the shift and broadening of transmission peaks and the spectral strength of specific surface roughness of individual samples. In addition, we have discussed the role of a thin overlayer in this respect. From this discussion, it appears that reducing the statistical uncertainties in probing the surface roughness can further improve the measurement resolution.

**ACKNOWLEDGEMENTS** The authors are grateful to the financial support by Multidisciplinary research program of the University Initiative (MURI) (Grant # N00014-01-1-0803), Office of Naval Research (ONR) Young Investigator award (Grant # N00014-02-1-0224), and National Science Foundation (NSF) CAREER Award, DMII: #9703426.

## Appendix

1) Derivation of the overall evanescent field in air/silver/glass configuration:

For given  $k_x$ , we have  $k_{zj} = \sqrt{\varepsilon_j \left(\frac{\omega}{c}\right)^2 - k_x^2}$  for  $j = 1$  (air) and  $j = 3$  (glass); and  $k_{z2} = +i\sqrt{k_x^2 - \varepsilon_1 \left(\frac{\omega}{c}\right)^2}$  for  $j = 2$  (silver).

The silver slab is placed in the region  $0 < z < d$  and we can solve the overall transmission and reflection coefficients using Fresnel equations:

$$R_p(123) = \frac{\left(\frac{k_{z1}}{\varepsilon_1} - \frac{k_{z2}}{\varepsilon_2}\right) \left(\frac{k_{z2}}{\varepsilon_2} + \frac{k_{z3}}{\varepsilon_3}\right) \exp(-ik_{z2}d) + \left(\frac{k_{z1}}{\varepsilon_1} + \frac{k_{z2}}{\varepsilon_2}\right) \left(\frac{k_{z2}}{\varepsilon_2} - \frac{k_{z3}}{\varepsilon_3}\right) \exp(ik_{z2}d)}{\left(\frac{k_{z1}}{\varepsilon_1} + \frac{k_{z2}}{\varepsilon_2}\right) \left(\frac{k_{z2}}{\varepsilon_2} + \frac{k_{z3}}{\varepsilon_3}\right) \exp(-ik_{z2}d) + \left(\frac{k_{z1}}{\varepsilon_1} - \frac{k_{z2}}{\varepsilon_2}\right) \left(\frac{k_{z2}}{\varepsilon_2} - \frac{k_{z3}}{\varepsilon_3}\right) \exp(ik_{z2}d)}; \quad (\text{A.1})$$

$$T_p(123) = \frac{4 \left(\frac{k_{z1}}{\varepsilon_1}\right) \left(\frac{k_{z2}}{\varepsilon_2}\right)}{\left(\frac{k_{z1}}{\varepsilon_1} + \frac{k_{z2}}{\varepsilon_2}\right) \left(\frac{k_{z2}}{\varepsilon_2} + \frac{k_{z3}}{\varepsilon_3}\right) \exp(-ik_{z2}d) + \left(\frac{k_{z1}}{\varepsilon_1} - \frac{k_{z2}}{\varepsilon_2}\right) \left(\frac{k_{z2}}{\varepsilon_2} - \frac{k_{z3}}{\varepsilon_3}\right) \exp(ik_{z2}d)}. \quad (\text{A.2})$$

(1) In the region  $z < 0$  (air):

$$H_y(z) = \exp(ik_{z1}z) + R_p(123) \exp(-ik_{z1}z); \quad (\text{A.3a})$$

$$E_x(z) = -\frac{k_{z1}}{\omega\varepsilon_1} [\exp(ik_{z1}z) - R_p(123) \exp(-ik_{z1}z)]; \quad (\text{A.3b})$$

(2) In the region  $0 < z < d$  (silver):

$$H_y(z) = B \exp(ik_{z2}z) + C \exp(-ik_{z2}(z-d)); \quad (\text{A.4a})$$

$$E_x(z) = \frac{-k_{z1}}{\omega\varepsilon_1} [B \exp(ik_{z2}z) - C \exp(-ik_{z2}(z-d))]; \quad (\text{A.4b})$$

(3) In the region  $z > d$  (glass):

$$H_y(z) = T_p(123) \exp(ik_{z2}(z-d)); \quad (\text{A.5a})$$

$$E_x(z) = \frac{-k_{z3}}{\omega\varepsilon_3} T_p(123) \exp(ik_{z3}(z-d)). \quad (\text{A.5b})$$

Note that a common factor  $A \exp(ik_x x - i\omega t)$  is implicit in this form.

By matching the boundary condition at interface  $z = 0$  and  $z = d$ , we can determine the coefficient  $B$  and  $C$  for field distribution in the slab:

$$B = \frac{1}{2} (1 + R_p) + \frac{1}{2} \frac{k_{z1}/\varepsilon_1}{k_{z2}/\varepsilon_2} (1 - R_p); \quad (\text{A.6a})$$

$$C = \frac{\exp(-ik_{z2}d)}{2} \left[ (1 + R_p) - \frac{k_{z1}/\varepsilon_1}{k_{z2}/\varepsilon_2} (1 - R_p) \right]. \quad (\text{A.6b})$$

## REFERENCES

- 1 J.B. Pendry: Phys. Rev. Lett. **85**, 3966 (2000)
- 2 H. Raether: *Surface Plasmons*, Springer-Verlag, Berlin (1988)
- 3 H. Raether: *Excitation of Plasmons and Interband Transitions by Electrons*, Springer-Verlag, Berlin (1980) Chapt. 10
- 4 E. Kretschmann: Z. Phys. **241**, 313 (1971)
- 5 E. Kroeger, E. Kretschmann: Z. Physik **237**, 1 (1970)
- 6 E. Kretschmann: Opt. Comm. **5**, 331 (1972)
- 7 D.R. Smith, D. Schurig, M. Rosenbluth, S. Schultz, S.A. Ramakrishna, J.B. Pendry: Appl. Phys. Lett. **82**, 1506 (2003)
- 8 S.A. Ramakrishna, J.B. Pendry, D. Schurig, D.R. Smith, S. Schultz: J. Mod. Optics **49**, 1747 (2002)
- 9 N. Fang, X. Zhang: Appl. Phys. Lett. **82**, 161 (2003)
- 10 E.T. Arakawa, M.W. Williams, R.N. Hamm, R.H. Ritchie: Phys. Rev. Lett. **31**, 1127 (1973)
- 11 R.W. Alexander, G.S. Kovener, R.J. Bell: Phys. Rev. Lett. **32**, 154 (1974)
- 12 D. Hornauer: Opt. Comm. **16**, 76 (1976)
- 13 I. Pockrand, H. Raether: Appl. Opt. **16**, 1784 (1977)
- 14 A.A. Maradudin, D.L. Mills: Phys. Rev. **B11**, 1392 (1975)
- 15 O.S. Heavens: *Optical Properties of Thin Solid Films*, Dover, Mineola (1991)
- 16 S. Hayashi, T. Kume, T. Amano, K. Yamamoto: Jpn. J. Appl. Phys. **35**, L331 (1996)
- 17 J. Moreland, A. Adams, P.K. Hansma: Phys. Rev. B **25**, 2297 (1982)
- 18 P.B. Johnson, R.W. Christy: Phys. Rev. B **6**, 4370 (1972)

- 19 Oriel Instruments, *The Book of Photon Tools*, (2002) Chapt. 15
- 20 J.J. Burke, G.I. Stegeman, T. Tamir: Phys. Rev. B **33**, 5186 (1986)
- 21 P. Dawson, B.A.F. Puygranier, J.-P. Goudonnet: Phys. Rev. B **63**, 205 410 (2001)
- 22 M. Born, E. Wolf (Eds.): *Principles of Optics*, Pergamon Press, fourth edn. (1970)
- 23 V.G. Veselago: Sov. Phys. Usp. **10**, 509 (1968)
- 24 R.A. Shelby, D.R. Smith, S. Schultz: Science **292**, 77 (2001)
- 25 H.J. Simon, J.K. Guha: Opt. Comm. **18**, 391 (1976)
- 26 J.B. Pendry: In *Photonic Crystals and Light Localization in the 21st Century*, ed. by C.M. Soukoulis, NATO Science Series (2001)
- 27 M. Kahl, E. Voges: Phys. Rev. B **61**, 14078 (2000)
- 28 J.C. Quail, J.G. Rako, H.J. Simon, R.T. Deck: Phys. Rev. Lett. **50**, 1987 (1983)
- 29 F. Moresco, M. Rocca, T. Hildebrandt, M. Henzler: Phys. Rev. Lett. **83**, 2238 (1999)
- 30 H.J. Lezec, A. Degiron, E. Devaux, R.A. Linke, L. Martin-Moreno, F.J. Garcia-Vidal, T.W. Ebbesen: Science **297**, 820 (2002)
- 31 R.W. Ziolkowski, E. Heyman: Phys. Rev. E **64**, 056 625 (2001)
- 32 N. Fang, Z. Liu, T.-J. Yen, X. Zhang: Opt. Exp. **11**, 682 (2003)
- 33 Z. Liu, N. Fang, T.-J. Yen, X. Zhang: Appl. Phys. Lett. **83**, 5184 (2003)